Proceedings of the 19th International Conference on Automation & Computing, Brunel University London, UK, 13-14 September 2013

Full Beam Atomic Force Microscopy.

Umar Khan
Department of Electronics and Computer Science
University of Southampton
Southampton SO17 1BJ
Email: uaak1g10@ecs.soton.ac.uk

Mark French
Department of Electronics and Computer Science
University of Southampton
Southampton SO17 1BJ
Email: mcf@ecs.soton.ac.uk

Harold Chong
Department of Electronics and Computer Science
University of Southampton
Southampton SO17 1BJ
Email: hmhc@ecs.soton.ac.uk

***Abstract*—This contribution reports a method for increasing the imaging speed of an Atomic Force Microscope. The is done by allowing the complete length of the cantilever beam to interact with the sample surface rather than just the free end. The deflection of the beam is then observed at uniformly distributed points along the beam length using an array of laser spots and detectors. This scheme enables measurement of an entire line on the sample surface simultaneously, thus eliminating the need for rastering and reducing imaging time. This speed up is illustrated in this contribution through simulation results.**

***Keywords*—Atomic Force Microscopy, High Speed Scanning**

I. Introduction

The development of Atomic Force Microscopes in 1986 by Binning *et.al* [1] initiated initiated the usage of this versatile instrument in a diverse range of fields ranging from material science to microbiology. One key factor behind their high applicability is that the sample does not need to be conducting as was the case for the predecessor instrument, the Scanning Tunnelling Microscope (STM). Additionally, the samples can be viewed in air, liquid or vacuum with little or no sample preparation.

Although highly applicable, this instrument has a key limitation i.e, the image generation process is relatively *slow*. Currently it takes half a minute to four minutes for generating a 256×256 pixel image of an approximately 20×20 μm area. The most important problem limiting AFM speed is that the piezo-actuators used for moving the sample include resonant modes in their dynamics.

A number of solutions have been proposed for reducing the imaging time in an AFM. These can be classified into four groups. The most direct method is to improve the design of the piezo- actuators that are used for rastering the sample. The primary effort in this direction of research is to increase the resonance frequency of the piezo-actuator so that rastering at higher frequencies may be possible. A few examples of this work include the high speed scanner proposed by Schitter *et.al* [2] and Ando *et.al* [3]. The former designs scanners with higher resonance frequencies using Finite Element Analysis and the later increases resonance frequencies by using a piezo support mechanism which the authors refer to as the *inertia balance support*.

The second body of research work aims to improve AFM scan speeds though optimal controller design so that the effect of the resonant modes in the piezo actuators is reduced. One of the most common approaches used to enable faster rastering is to use H_∞ control theory for designing compensators [4] and estimators [5]. Substantial speed-ups can be obtained using this method as has been reported in [6]. An alternate method used to enable faster rastering is to identify a model of the piezo-actuator and compensate for the dynamics of the actuator that cause image distortion using feedforward control based model inversion. Burns [7] reports the usage of this strategy for high speed imaging on a Multi Mode AFM from Bruker. A similar method has been reported by Ando [8] for imaging biomolecules.

Another possibility for reducing imaging times is to optimize the imaging trajectories so that the resonant modes of the piezo actuators may not be excited. This is done by using scan trajectories with reduced harmonic content as reported in [9], [10].

Lastly, a few researchers have experimented with a complete workaround the entire problem of the piezo actuator resonant modes. This is achieved by using an array of parallel cantilevers [11] to reduce the imaging time. The approach proposed in this contribution is similar to this method except that instead of using multiple cantilevers, the beam is pinned at both ends and is moved laterally over the entire surface. The beam is assumed to have multiple tips distributed uniformly over the entire beam length. This allows the beam to interact with the sample surface at multiple points thus enabling faster imaging. The beam deflection is then observed using an array of laser spots also distributed uniformly across the beam length. This information is used to estimate the topography of the surface. A control loop is also used to ensure that the entire sample surface remains within an acceptable distance from the beam tips. As illustrated in section V, the speed-up attained using this method determined by the resonance frequency of the piezo actuator used to move the sample. Given the specifications of current piezo actuators, it is illustrated that a speed up in excess of five hundred times can be obtained. The primary advantage of this method over the use of multiple cantilevers is the relatively simpler construction. Instead of using multiple cantilevers only one beam is needed. Secondly, only one feedback control loop is needed which vastly simplifies implementation.

Current state of the art AFMs have scan rates well in excess of 10 Hz as in the case of [12] and [13], however

the principle of full beam atomic force microscopy also applies to these instruments.

The remaining parts of the paper are organized as follows, section II explains the fundamentals of AFM operation, section III describes the set up for the full beam atomic force microscopy followed by an explanation of the control law in section IV. Section V provides the simulation results for a simple uniform rectangular grid, followed by the conclusions and future work in the last section.

II. AFM Fundamentals

Figure 1 illustrates the setup of a conventional AFM which consists of a cantilever, laser source, photo diode and a piezo tube actuator on which the sample is placed. Generally the cantilever is made of silicon nitride, silicon oxide or silicon and is up to 250 μm in length. A pyramid shaped tip is attached to the free end of the cantilever facing the sample surface. This tip is nearly atomically sharp and is used to probe the sample.

The interaction between the tip and sample causes the cantilever to deflect. This deflection is detected by shining a laser beam on top of the cantilever's free end and detecting the deflection using a Photo Sensitive Diode (PSD). The sample is then rastered beneath the cantilever tip. This is done by actuating the piezo tube on which the sample rests. The piezo tube has the ability to bend laterally in the x and y directions, and contract and expand to provide movement vertically in the z direction. The piezo actuation in the lateral directions is achieved by providing triangular voltage waveforms V_x and V_y with frequencies f_x and f_y respectively. Each change of the V_x voltage from one extreme to the other corresponds to one scan line. Consecutive scan lines are referred to as the *trace* and *retrace* scan lines. The change in the V_y from one extreme to the other corresponds to one image frame. In most conventional AFMs, the frequency for the x axis, which is also referred to *fast* axis is below 10 Hz and each image consists of 256 trace and retrace line pairs. Higher scan frequencies have been reported, but currently most conventional AFMs are restricted below this limit. The problem associated with higher scan frequencies is that these excite the resonant modes of the piezo actuators which cause distortions in the image.

Given that $f_x = 10$ Hz an image consists of 256 trace retrace line pairs, the time required for each image T_{image} is 25.6 seconds. The scan rate for the y axis f_y is then selected so that its time period is twice T_{image}, i.e, $f_y = \frac{1}{2 \times T_{image}}$.

As the sample is rastered beneath the cantilever tip, the cantilever tip deflection changes as a consequence of variations in surface topography. These changes are observed by measuring the photo sensitive diode's (PSD) voltage signal d. The purpose of the control loop is then to regulate the height of the sample so that the deflection signal d remains at it's set point d_{SP}. The movement is achieved by adjusting the V_z which corresponds to the vertical movement of the piezo tube.Finally, the controller signal h provides an estimate of the sample topography.

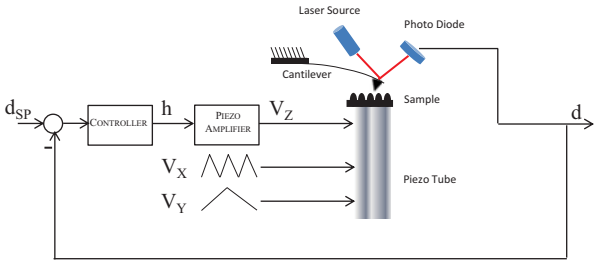

Figure. 1. Atomic Force Microscope setup.

III. Full Beam Atomic Force Microscopy

The fundamental principle of the *Full Beam* atomic force microscopy is to use the entire length of the cantilever for determining the topography of the sample. As illustrated in Figure 2 the beam consists of N_T tips distributed uniformly across it's length. Contrary to conventional atomic force microscopy where beam is fixed at one end and free at the other, in this case the beam is pinned at both ends to a fixed support. The sample is placed on a piezo actuator at a distance Z_c below the pinned ends of the beam. The piezo actuator enables both lateral and vertical movement of the sample.

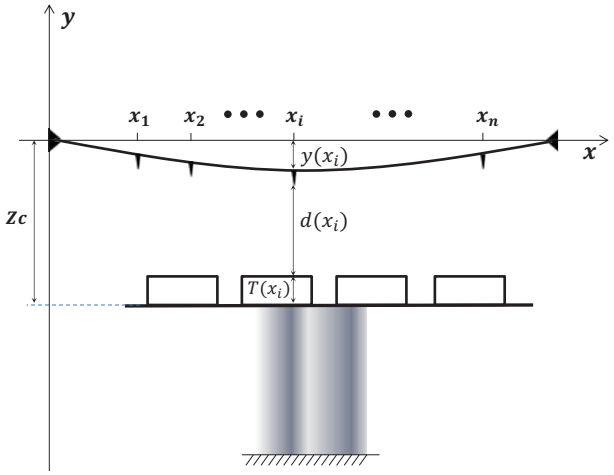

Figure. 2. Full Beam Atomic Force Microscope setup.

The top end of the beam above each tip is illuminated with N_S laser spots that enables measurement of the deflection angle of the beam $\theta_i = \frac{d\theta}{dx}\big|_{x=x_i}$ for the i^{th} tip. For the purpose of the current contribution $N_T = N_S = n$. The vector of deflection angles $\vec{\theta} = [\theta_1 \ \theta_2 \ \dots \ \theta_n]^T$ is used to evaluate the vector of forces and moments acting on the beam at the location of each tip $\vec{F} = [f_1 \ \tau_1 \ \ f_2 \ \tau_2 \ \ \dots \ \ f_n \ \tau_n]^T$. Here f_i is the tip sample interaction force acting on the i^{th} tip and τ_i is the moment acting on the beam at the location of each tip.

Once the force vector is known the sample topography can be estimated by inverting the tip sample interaction relation. This places two constraints on the full beam AFM set up given below,

$$a_o \leq |d(x_i)| \leq d_{max} \quad \forall\, 1 \leq i \leq n \tag{1}$$
$$|T(x_i)| \leq d_{max} \quad \forall\, 1 \leq i \leq n \tag{2}$$

Here a_o is the inter atomic separation for the sample material. It is the closest distance the tip can be from the sample surface without penetrating it. d_{max} is the maximum separation between the tip and sample after which the effect of the tip sample interaction force is too small to be measured. The motivation behind placing this constraint is to ensure that the tip sample interaction force is explained solely by the Van der Waals interaction force between tip and sample. The second constraint is a simple extension of the first one. If the sample topography has a variation greater than d_{max} then either some regions of the sample surface will be too far to exert any measurable force on the beam, or the tips will penetrate the sample. In both cases topography reconstruction will become impossible. The complete tip sample interaction force is explained by the following relation,

$$f_i = \begin{cases} -\frac{HR}{6d_i^2} & \text{if } d_i > a_o \\ -\frac{HR}{6a_o^2} + \frac{4}{3}E^*\sqrt{R}(a_o - d_i)^{\frac{3}{2}} & \text{if } d_i \leq a_o. \end{cases} \tag{3}$$

where $d_i = d(x_i)$ H is the Hammaker constant, R is the tip radius, E^* is the effective Young's Modulus. Figure 3 illustrates one possible tip sample interaction force curve for $E^* = 1.3$ GPa, $R = 10$ nm, $a_o = 0.16$ nm and $H = 7.1 \times 10^{-20}$ J.

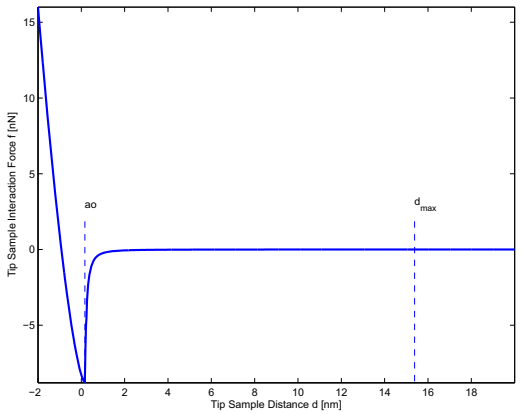

Figure. 3. Tip sample interaction force.

As is clear from Equation 3 if the tip sample distance is greater than a_o the interaction force is explained by a single term which is the Van der Waals force. If the distance is less than a_o i.e, the tip starts penetrating the surface and the interaction force is explained by an additional term originating from the Derjaguin Muller Toporov (DMT) model [14]. In this case d_{max} is determined by using the fact that current AFMs can measure a minimum force F_{min} of 1 pico Newtons [15] and then inverting the Van der Waals relation i.e, $d_{max} = \sqrt{\frac{-HR}{6 \times F_{min}}}$. Here the negative sign in the root is not a problem since the Van der Waals force always cause the tip to be attracted towards the surface thus giving F_{min} a negative sign as well. For the current values of H and R, $d_{max} = 15.38$ nm.

Finally the complete topography estimation process can be given as a mapping Φ,

$$\Phi : map\ \theta_i \rightarrow (f_i, y_i) \quad \forall\, 1 \leq i \leq n \tag{4}$$

Where $y_i = y(x_i)$ is the beam deflection at $x = x_i$. Once the tip forces and beam deflections are known, the topography can be determined by the using the following relation obtained from Figure 2,

$$T_i = |y_i - Zc| - |d_i| \quad \forall\, 1 \leq i \leq n \tag{5}$$

Where $T_i = T(x_i)$ is the topography at $x = x_i$. Using the constraints which ensure that the tip sample interaction force is explained only by the Van der Waals force, this relation becomes,

$$T_i = |y_i - Zc| - \sqrt{\frac{-HR}{6 \times f_i}} \quad \forall\, 1 \leq i \leq n \tag{6}$$

The mapping Φ can be obtained by using the Finite Element Model (FEM) for the beam. This is done by using the FEM matrices for the beam namely *Mass*, *Damping* and *Stiffness* matrices M,C and K respectively. The complete matrix equation for the systems can then be written as,

$$M\ddot{\vec{X}} + C\dot{\vec{X}} + K\vec{X} = \vec{F} \tag{7}$$

where $\vec{X} = [y_1\ \theta_1\ \ y_2\ \theta_2\ \ \dots\ \ y_{n+1}\ \theta_{n+1}]^T$, $\vec{F} = [f_1\ \tau_1\ \ f_2\ \tau_2\ \ \dots\ \ f_{n+1}\ \tau_{n+1}]^T$ and n is the number of elements in the finite element model. The mass, damping and stiffness matrices can be constructed by using the corresponding mass, stiffness and damping matrices for each element namely M_i, C_i and K_i and matrix assembly procedure. The element matrices used in this contribution are obtained from [16] and are given below,

$$M_i = \frac{mL}{420n}\begin{bmatrix} 156 & 22 & 54 & -13 \\ 22 & 4 & 13 & -3 \\ 54 & 13 & 156 & -22 \\ -13 & -3 & -22 & 4 \end{bmatrix} \quad i = 1, 2, \dots, n \tag{8}$$

$$K_i = \frac{EIn^3}{L^3}\begin{bmatrix} 12 & 6 & -12 & 6 \\ 6 & 4 & -6 & 2 \\ -12 & -6 & 12 & -6 \\ 6 & 2 & -6 & 4 \end{bmatrix} \quad i = 1, 2, \dots, n \tag{9}$$

Where, m is the mass per unit length for the beam, E is the Elasticity Modulus, I is the moment of inertia through the transverse axis and L is the beam length. The element matrices are assembled using the assembly procedure mention in [16] to obtain M and K. Once these

are obtained, the stiffness matrix C is determined as a linear combination of M and K using Rayleigh Damping.

Assuming that $\ddot{\vec{X}}$ and $\dot{\vec{X}}$ are negligible we get,

$$K \begin{bmatrix} y_1 \\ \theta_1 \\ y_2 \\ \theta_2 \\ \vdots \\ y_{n+1} \\ \theta_{n+1} \end{bmatrix} = \begin{bmatrix} f_1 \\ \tau_1 \\ f_2 \\ \tau_2 \\ \vdots \\ f_{n+1} \\ \tau_{n+1} \end{bmatrix} \tag{10}$$

This assumption is reasonable if the beam is allowed to settle to a steady state before the topography estimation can begin.

The purpose of the mapping Φ is to use the known values of the measured deflection angles $\theta_1\ \theta_2\ \dots\ \theta_{n+1}$ and determine $f_1\ f_2\ \dots\ f_{n+1}$ and $x_1\ x_2\ \dots\ x_{n+1}$. It is already known that while the tip sample interaction exerts forces on the tip but no moments, i.e $\tau_1 = \tau_2 \cdots = \tau_{n+1} = 0$.

The system of equations 10 is rearranged using a permutation matrix P as follows,

$$P \begin{bmatrix} y_1 \\ \theta_1 \\ y_2 \\ \theta_2 \\ \vdots \\ \vdots \\ y_{n+1} \\ \theta_{n+1} \end{bmatrix} = \begin{bmatrix} y_1 \\ y_2 \\ \vdots \\ y_{n+1} \\ \hline \theta_1 \\ \theta_2 \\ \vdots \\ \theta_{n+1} \end{bmatrix} = \vec{\vec{X}} \tag{11}$$

and using the same permutation matrix,

$$P \begin{bmatrix} f_1 \\ \tau_1 \\ f_2 \\ \tau_2 \\ \vdots \\ \vdots \\ f_{n+1} \\ \tau_{n+1} \end{bmatrix} = \begin{bmatrix} f_1 \\ f_2 \\ \vdots \\ f_{n+1} \\ \hline \tau_1 \\ \tau_2 \\ \vdots \\ \tau_{n+1} \end{bmatrix} = \vec{\vec{F}} \tag{12}$$

This permutation matrix is then used to determine the rearranged system of equations as follows,

$$KP^{-1}P\vec{\vec{X}} = P^{-1}P\vec{\vec{F}} \tag{13}$$

$$PKP^{-1}\vec{\vec{X}} = \vec{\vec{F}} \tag{14}$$

$$\bar{K}\vec{\vec{X}} = \vec{\vec{F}} \tag{15}$$

The matrices $\bar{K}$, $\vec{\vec{X}}$ and $\vec{\vec{F}}$ are partitioned as follows,

$$\begin{bmatrix} K_{yy} & K_{y\theta} \\ K_{\theta y} & K_{\theta\theta} \end{bmatrix} \begin{bmatrix} \vec{y} \\ \vec{\theta} \end{bmatrix} = \begin{bmatrix} \vec{f} \\ \vec{0} \end{bmatrix} \tag{16}$$

Where $\vec{y} = [y_1\ \ y_2\ \ \dots\ \ y_{n+1}]^T$ and $\vec{\theta} = [\theta_1\ \theta_2\ \dots\ \theta_{n+1}]^T$ and $\vec{f} = [f_1\ f_2\ \dots\ f_{n+1}]$. Finally, $\vec{y}$ can be determined as follows,

$$\vec{y} = -K_{\theta y}^{-1} K_{\theta\theta} \vec{\theta} \tag{17}$$

Once $\vec{y}$ is known, $\vec{f}$ is determined using Equation 16.

IV. Full Beam AFM Control Loop

Contrary to the conventional AFM control loop where the AFM plant where both the control and error signals are time dependent scalars, the full beam AFM requires regulating the sample height Z_c as illustrated in Figure 2 to keep the vector of deflection angles $\vec{\theta}$ at a set point vector $\vec{\theta}_{sp}$. The error signal is therefore a vector given as,

$$\vec{e} = \vec{\theta}_{sp} - \vec{\theta} \tag{18}$$

The set point vector θ_{sp} is selected so that all points along the beam length stay in the desired region between a_o and d_{max}, i.e,

$$a_o \leq y_i \leq d_{max} \quad \forall\ 1 \leq i \leq n \tag{19}$$

This done by setting Zc to an arbitrarily chosen value between a_o and d_{max} (in this contribution $Z_c = -10$ nm), letting the surface be flat simulating the beam motion using Equation 7. The beam is assumed to be at rest initially and moves under the influence of the tip sample interaction force. Eventually, the beam attains a steady state so that $\ddot{\vec{y}} = \dot{\vec{y}} = \ddot{\vec{\theta}} = \dot{\vec{\theta}} = 0$. The value of $\vec{\theta}$ is used as the set point $\vec{\theta}_{sp}$.

The fact that the error signal is a vector gives rise to two problems. Firstly, it needs to be determined how *far* the vector $\vec{\theta}$ is from the set point vector $\vec{\theta}_{sp}$. Secondly, given a measure of how far $\vec{\theta}$ is from $\vec{\theta}_{sp}$, it must also be determined if the sample needs to be moved towards the beam or away from it.

While the problem of the distance metric can be solved by using the L_2 norm of the error signal vector as done in this contribution, the second problem requires utilization of the beam geometry. This is illustrated in Figure 4. The figure shows the beam deflections y_i, deflection angles θ_i and the corresponding errors e_i when the beam is too close to a flat surface, when it is at a distance where $\vec{\theta} = \vec{\theta_{sp}}$ and when it is too far from the surface. For the purpose of this illustration, the figure was generated by setting Z_c = 8,10 and 12 nm respectively.

The top plot in Figure 4 illustrates the beam deflections for the three cases. As is clear from the plot, the beam shows greater deflection when closer to the surface because the magnitude of the tip sample interaction force is greater. Likewise the beam exhibits lesser deflection when farther away from the surface. The middle plot illustrates the deflection angles. For the first half of the beam before the middle point the deflection angles are all negative since the beam has a negative slope in this region. Likewise the slopes are positive for the second

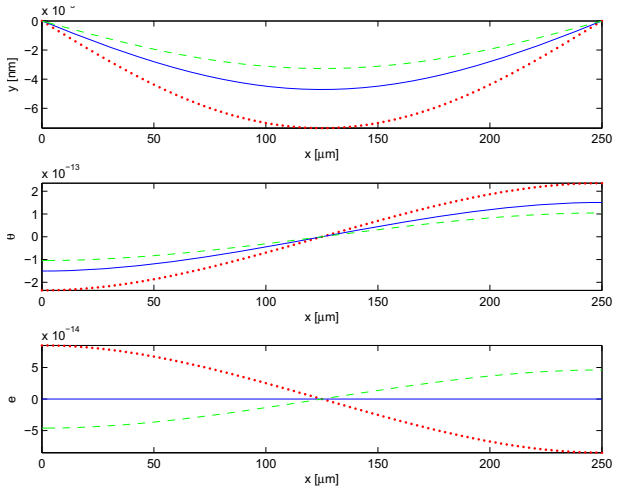

Figure. 4. Determination of the error metric for three beam positions, near(..), at setpoint (–) and far(- -).

half of the beam. The third plot illustrates the deflection angle error. It is can be seen clearly that if the beam is too close to the surface the error values are positive for the first half of the beam and then negative and vice versa. This metric if given as follows,

$$E = sgn\left(\sum_{i=1}^{0.5(n+1)} e_i - \sum_{i=0.5(n+1)+1}^{n+1} e_i\right)|\vec{e}|_2^2 \qquad (20)$$

The first term involving the signum function indicates if the surface needs to be moved towards the beam or away from it. The second term involving the L_2 norm is simply used to measure the size of the error. Finally, the controller attempts to minimize $E(t)$ by regulating the sample height Z_c. This contribution reports the results of using a simple Proportional controller along with a first order low pass filter to minimize oscillations in Z_c. These results are reported in the next section.

V. Simulation Results

This section presents simulation results for the case when the sample is moved laterally at a uniform velocity so that the topography of the entire surface may be estimated. The system is simulated by using the finite element model given in Equation 7. This is done by converting the M,C and K matrices into the corresponding state space matrices for the system.

The system is then simulated with a sample time of $T_s = 0.2\mu s$. The finite element model consists of $N_E = N_T = N_S = n = 100$ finite elements. Table I illustrates the all the remaining simulation parameters for the sample and the beam.

The initial conditions for the beam are set to zero and Z_c is set to -15nm. For the purpose of this contribution $f_x = 0$ and $f_y = 10$ Hz. The sample surface in this case is a rectangular grid with pitch of $100\mu m$ and a height of 5 nm. The image covers an area of $250 \times 500\mu m$. Given the scan rate f_y, 0.1 seconds are required for recording the image.

TABLE I. Simulation Parameters for Full Beam Scan Simulation

	Parameter	Value
Sample	Pitch	100 μm
	Height	5 nm
	Hammaker Constant (H)	7.1 $\times 10^{-20}$ J
	Inter-atomic Separation (a_o)	0.16 nm
	Young's Modulus (E_s)	1.2 GPa
	Poisson's Ratio (ν_s)	0.3
Beam	Tip Radius (R)	20 nm
	Young's Modulus (E_b)	130 GPa
	Poisson's Ratio (ν_b)	0.3
	Beam Length (L)	250 μm
	Beam Width (w)	35 μm
	Beam Thickness (t)	3 μm
	Number of Tips (N_T)	100
	Number of Spots (N_S)	100
Simulation	Sample Time (T_s)	0.2 μs
	Number of Beam Elements (N_E)	100

If conventional AFM imaging is used with 512 trace retrace line pairs and a scan rate $f_x = 10$ Hz, 51.2 seconds would be needed to complete the scan. The full beam scanning in this case is therefore 512 times faster. It is clear that while the speed-up factor may vary for different values of f_x and for a different number of trace retrace line pairs, the full beam method will always be faster than conventional AFM imaging. This is because in conventional AFM a single tip must be moved sequentially over the sample where as in this method a large number of tips are moved over the surface in parallel.

Figure 5 illustrates the results of the topography reconstruction. As can be seen that the sample surface is reasonably estimated, although there are distortions near the edges. This is due to the fact that since the sample topography is constantly changing, the assumption that $\ddot{\vec{X}}$ and $\dot{\vec{X}}$ are negligible is no longer true. This causes inaccuracies in estimation of the sample surface. Due to this reason, the topography estimates either exceed d_{max} or are lesser than a_o at some points. Such estimates are discarded from the final result. Despite these errors an acceptable reconstruction is still obtained.The error and controller signals are illustrated in Figure 6. The error signal oscillates initially (as shown in inset) and then converges to zero.

VI. Conclusions

This contribution presents a possible solution for reducing imaging times in atomic force microscopes. The fundamental concept is to use the entire length of the cantilever beam rather than only the free end. The advantage is that samples can be scanned faster. There are also implementation challenges that need to be investigated to enable realization of this concept. The first one is the fabrication of a large number of tips on the entire beam length. This would require that each tip have a high aspect ratio and a base length less than a micro meter, as is the case with AFM probe tips from nanoScience Instruments [17]. The current simulation assumes the fabrication of 100 tips on a 250 μm beam. The second implementation issue requiring investigation is the placement of a large number of laser spots on the beam. One possible solution

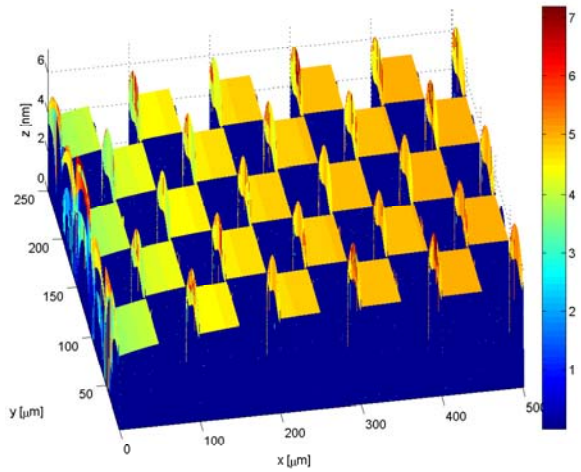

Figure. 5. Topography reconstruction for two dimensional scan.

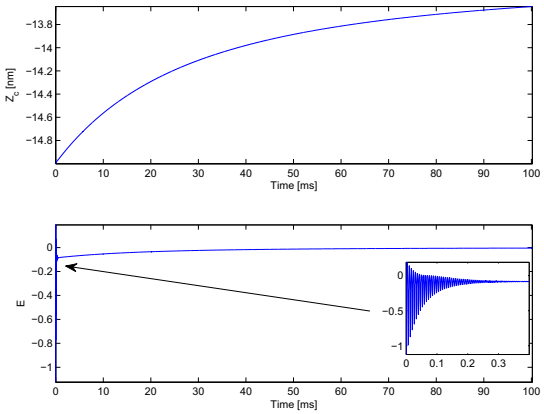

Figure. 6. Control signal Z_c (top). Error signal E (bottom).

is to use self sensing piezo resistive mechanisms as have been suggested in [18]. Instead of using a single piezo resistive element, an array could be fabricated on the entire beam length to eliminate the requirement for optical detection.

An additional implementation difficulty is the requirement of parallel sampling of large number of channel at a very high sampling rate in excess of 1×10^6 samples per second. This clearly exceeds the capabilities of a large number of low cost off the shelf data acquisition devices and would necessitate the development of analogue circuitry which can obtain the scalar error signal E from the error vector $\vec{e}$.

Lastly, the constraints assumed for maximum sample topography variation may appear restrictive, however a number of samples of practical interest exhibit topography variations that fall well within this range. One example is the viewing of biological samples for instance DNA at a high frame rate. This is important since this can lead to a better understanding of biological processes at a molecular scale. Earlier Ando *et.al* observed the motion of a Myosin V protein molecule using a high speed AFM, which improved the understanding of such motion mechanisms. In this context the development of a mechanism that uses the complete length of the cantilever beam for interacting with the surface will lead to even faster imaging and a better study of biological samples.

REFERENCES

[1] G. Binning, C.F. Quate and Ch. Gerber, "Atomic Force Microscope", Physical Review Letters, 1986, pp. 930.

[2] G. Schitter, G. E. Fantner, P. J. Thurner, J. Adams and P. K. Hansama, "Design and characterization of a novel scanner for high-speed atomic force microscopy", 4^{th} IFAC Symposium on Mechatronics, 2006.

[3] T. Fukuma, Y. Okazaki, N. Kodera, T. Uchihashi and T. Ando, "High resonance frequency force microscope scanner using inertia balance support", Applied Physics Letters, 92, 243119, 2008.

[4] A. Sebastian, "Nanotechnology: A Systems and Control Approach", Ph.D. Dissertation, Department of Electrical Engineering, Iowa State University, 2004.

[5] S. M. Salapaka and M. V. Salapaka, "A control systems perspective on nanointerrogation", IEEE Control Systems Magazine, 2008.

[6] C. Lee, S. M. Salapaka, "Two degree of freedom control for nanopositioning systems: Fundamental limitations, control design and related trade-offs", American Control Conference, 2009.

[7] D. J. Burns, "A system dynamics approach to user independence in high speed microscopy", Ph.D. Dissertation, Department of Mechanical Engineering, 2010.

[8] N. Kodera, D. Yamamoto, R. Ishikawa and T. Ando, "Video imaging of walking myosin V by high-speed atomic force microscopy", Nature, 2010, pp.72-76

[9] A. J. Fleming, A. G. Wills, "Optimal input signals for band limited scanning systems", Proceedings of the 17^{th} World Congress The International Federation of Automatic Control, 2008.

[10] A. Bazaei, Y. K. Yong, S. O. R. Moheimani, "High speed Lissajous-scan atomic force microscopy: Scan pattern planning and control design issues", Review of Scientific Instruments, 83, 063701, 2012.

[11] A. Schneider, R. H. Ibbotson, R. J. Dunn and E. Huq, "Arrays SU-8 microcantilevers with integrated piezoresistive sensors for parallel AFM applications", Microelectronic Engineering, 88 pp. 2390-2393, 2011.

[12] "World's Ultimate AFM, The new benchmark for speed with highest resolution and performance", Bruker, http://www.bruker.com/fastscan

[13] "The Cypher Atomic Force Microscope The Highest Resolution Fast Scanning AFM, The Highest Resolution Fast Scanning AFM", Asylum Research, http://www.asylumresearch.com

[14] B. V. Derjaguin, V. M. Muller, Y. P. Toporov, "Effects of contact deformations on the adhesion of particles", Journal of Colloid and Interface Science, vol. 53, pp. 314, 1975.

[15] P. J. Cumpson, J. Hedley and P. Zhdan, "Accurate force measurement in the atomic force microscope: a microfabricated array of reference springs for easy cantilever calibration", Nanotechnology, vol. 14, no. 8, 2003.

[16] L. Meirovitch, "Fundamentals of Vibrations", McGraw Hill, 2001.

[17] High Aspect Ratio - Pyramidal Silicon Tips, "NanoScience Instruments", [Online]. Available: http://store.nanoscience.com

[18] G. E. Fanter, D. J. Burns, A. M. Belcher, I. W. Rangelow and K. Y. Toumi, "DMCMN: In depth characterization and control of AFM cantilevers with integrated sensing and actuation", Journal of Dynamic Systems, Measurement and Control, vol. 131, 2009.